Theoretical Study of Porous Silicon Waveguides and Their Applicability for Vapour Sensing

Tanya Hutter*[1], Nikos Bamiedakis[2] and Stephen R. Elliott[1]
[1]Department of Chemistry, [2]Department of Engineering, University of Cambridge, UK
*Corresponding author: Lensfield Road, Cambridge CB2 1EW, UK, tf269@cam.ac.uk

Abstract: The finite-element method (FEM) (Comsol RF Module) has been employed for modal analyses of porous silicon (PSi) waveguides composed of a guiding layer of low porosity (high refractive index) on a cladding layer with higher porosity (lower refractive index). These can be made by switching the current density from a lower to a higher value during the electrochemical etching process. The applicability of these structures for vapour sensing is investigated and an extremely sensitive PSi-microring resonator is presented.

Keywords: porous silicon waveguide, mode analysis, FEM, sensor.

1. Introduction

Porous silicon (PSi) is typically produced by electrochemical etching of bulk crystalline silicon. The porosity of the produced material is directly proportional to the applied current density during the etching process, providing therefore a simple means to control its refractive index [1]. Various optical components such as Bragg and rugate reflectors have been successfully fabricated with porous silicon [2]. Porous silicon is compatible with silicon-based processing technologies and can thus be readily integrated with silicon-based devices.

Porous silicon is widely used for sensing, and in particular in vapour sensing, due to its large surface area and the capillary condensation phenomenon [3]. In this phenomenon, organic vapours condense inside the pores, causing a substantial and fully-reversible increase in the refractive index of the porous layer [3]. In addition, the surface of the porous silicon can be chemically modified to be sensitive to a specific analyte [4]. Buried PSi waveguides [5-7] are particularly attractive structures for use in sensing applications as they can be modified *in situ* either by exposing them to vapours or by introducing different materials such as solvents or dyes into their pores. For such structures, it has been shown that organic solvents change reversibly the intensity of the guided mode [8], while the organic dyes can be employed to exploit their non-linear optical properties [6, 9]. Such sensing devices fabricated from porous silicon can exhibit an improved sensitivity over devices made of different materials owing to their unique porous nature that provides a larger sensing surface area.

In this work, we present a theoretical study of porous silicon rib waveguides using the Comsol Multiphysics RF Module. The guided modes of the PSi structures are found, and their dispersion curves are investigated. Moreover, the effect of introduction of organic solvents into the waveguide pores on the waveguide modes is studied. Finally, a ring resonator based on PSi waveguides is presented and its optical transmission characteristics investigated. The proposed device exhibits high sensitivity of 700 nm per change of one unit in the refractive index of the surrounding medium.

2. Theory

2.1 Capillary condensation

The number of molecules that can be adsorbed by a porous layer is limited by the total pore volume. The pores' curved surfaces enhance the attraction for molecules of wetting substances due to van der Waals interactions, resulting in adsorption and capillary condensation. Capillary condensation is the physical tendency for a vapour to condense in a small pore at temperatures well above the dew point, and it described by the Kelvin equation:

$$N_A kT \ln(\frac{P}{P_0}) = -\frac{2M\gamma\cos\theta}{r\rho} \quad (1)$$

where N_A is Avogadro's constant, k is the Boltzmann constant, T is the absolute temperature, M is the molecular weight, ρ is the liquid density, r is the radius of the capillary, θ is the contact angle, γ is the surface tension, P_0 is the saturation pressure and P is the equilibrium vapour pressure. Therefore, the smaller the pore

radius, the lower the relative vapour pressure at which capillary condensation can occur at a given temperature. During the capillary condensation process, the air in the voids is replaced by condensed vapour. The extent of both the monolayer adsorption and the capillary condensation are influenced by the surface affinity of the porous matrix, which can be tailored to a range of chemical modifications [10].

The dielectric constant of the PSi layer undergoes a significant change when vapours diffuse to the inner regions of the pore structure. It has been shown that for water vapour, pore sizes between 1 to 30 nm in diameter are necessary to allow adequate condensation [11]. Several humidity sensors based on capillary condensation phenomenon have been proposed in the literature, some designed to detect humidity through changes of the capacitance [12, 13], or the optical properties of PSi layer [14].

2.2 Optical Properties of Porous Silicon

The refractive index of PSi is lower than of that bulk silicon due to the presence of air in the material pores, and it decreases with increasing porosity. For porous materials, the Bruggeman effective-medium approximation can be used in order to estimate their refractive index [15]. When porous silicon is exposed to analytes in the gas phase, capillary condensation causes an increase of its effective refractive index, as the air (n = 1) in the pores is replaced by the condensed analyte vapour (n > 1). By measuring the peak shifts in the reflection spectrum of the PSi after exposure to vapours, various chemical substances can be detected [16-19] and binary mixture compositions can quantitatively be characterised [20, 21].

A quantitative model accounting for the condensed vapours in the material pores can be realized by applying the Bruggeman effective-medium approximation theory, assuming that, after exposure at equilibrium, the chemical vapours fill a fraction V of the pores' volume p according to the equation:

$$(1-p)\frac{\varepsilon_{Si}-\varepsilon_{PSi}}{\varepsilon_{Si}+2\varepsilon_{PSi}}+(p-V)\frac{\varepsilon_{air}-\varepsilon_{PSi}}{\varepsilon_{air}+2\varepsilon_{PSi}}+ \qquad (2)$$

$$+V\frac{\varepsilon_{vap}-\varepsilon_{PSi}}{\varepsilon_{vap}+2\varepsilon_{PSi}}=0$$

where parameter p is the layer porosity, ε_{Si} and ε_{air} are the dielectric functions of Si and the air, V is the liquid fraction of the condensed vapour, ε_{vap} is the dielectric function of the embedding vapour and ε_{PSi} is the dielectric function for the porous layer.

2.3 Waveguide Sensors and Ring-Resonators

Light can couple into the guided modes of a waveguide and propagate over significant distances, depending on the material optical absorption and propagation loss at a specific wavelength. Evanescent-field waveguide sensors are based on the interaction of the guided light with the surrounding environment: the evanescent field of the guided modes is used to detect any changes in the optical properties of the cladding material, as for example the binding of molecules to the waveguide surface.

Ring resonators are commonly used as sensing elements to detect changes in the refractive index of the materials in close proximity (i.e. a coating of the waveguide surface or receptors attached to their surface). Their basic design consists of a bus waveguide in closely positioned next to a ring waveguide. Light from the bus waveguide can be strongly coupled into the ring structure if the phase-matching condition between the modes of the two structures is satisfied for a specific wavelength λ_i :

$$n_{eff} \cdot L = m \cdot \lambda_i \qquad (3)$$

where n_{eff} is the effective refractive index of the waveguide mode in the ring, L is the length of the ring, and m an integer. Resonant (phase-matching) conditions result in a sharp dip in the transmission spectrum of the bus waveguide as a large portion of the propagating optical power is stored in the ring structure. The binding of molecules to the ring-resonator waveguide surface changes the n_{eff} of the guided mode, and therefore results in a shift of the wavelength at which the resonance occurs.

PSi ring resonators can offer higher sensing sensitivity when compared with ring resonators made from other materials, as they provide the unique advantage that the presence of specific molecules changes the refractive index of the core material rather than that of the cladding. The change induced in the effective refractive index of the guided mode due to the presence of

the analyte is much larger than that caused by a change in the refractive index of the cladding material.

3. Simulation, Results and Discussion

3.1 Porous Silicon Fabrication, Morphology and Optical parameters

The fabrication procedure of porous silicon can be found in [22]. Samples were prepared using p-type doped silicon substrates with a resistivity of 0.01-0.02 Ω-cm and (100) crystal orientation. The silicon wafer was electrochemically etched using an electrolyte solution containing 30% HF (48% aqueous) and 70% ethanol. The current density and the etching times were taken and calculated, respectively, from [23] depending on the porosity and the thickness required. The thickness of the layers was determined by the time for which the current was applied. As the refractive index is determined by the applied current density, it is possible to design multi-layered structures and graded-index planar waveguides in which the porosity is varied through the vertical cross section of the structure. Silicon can spontaneously oxidize in air, and therefore the optical properties of such structures may change with time. In order to prevent the structure from uncontrolled oxidation after the fabrication, PSi samples can be thermally oxidized, in order to transform all silicon to silica.

The morphology of a fabricated porous silicon layer with 62% porosity on silicon can be seen in the recorded SEM image shown in Fig. 1a. Fig. 1b displays a magnification of the porous fractal structure, while Fig. 1c presents a top view of the porous silicon sample. It should be noted that pore-size distribution within the material volume does not significantly affect its optical properties since the pores, about 20 nm in diameter, are much smaller than the wavelength of light used (1.55 μm). The porous silicon layer can thus be considered as an effective medium with a refractive index that depends on the average porosity, and lies between the indices of silicon and air.

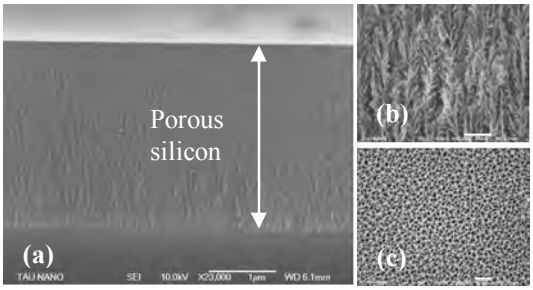

Figure 1. (a) HRSEM cross section view of pore morphology, (b) magnification and (c) top-view of the porous silicon surface. The scale bars are 1 μm and 100 nm.

The refractive indices of porous silicon layers of different porosity and exposed to different solvents are calculated using the Bruggeman effective-medium approximation theory. The refractive indices for the solvents are taken from [16], while the refractive index of silicon and silica are taken to be 3.48 and 1.44, respectively. The calculated refractive index of the porous layer as a function of the liquid-filling fraction at different solvent exposures is shown in Fig. 2a for 62% and in Fig. 2b for 75% porosity, respectively. Note that the higher the porosity, the lower the refractive index of the porous layer. In the theoretical studies in the remaining of the paper, the core is considered to have a 62% porosity while the cladding a 75% porosity.

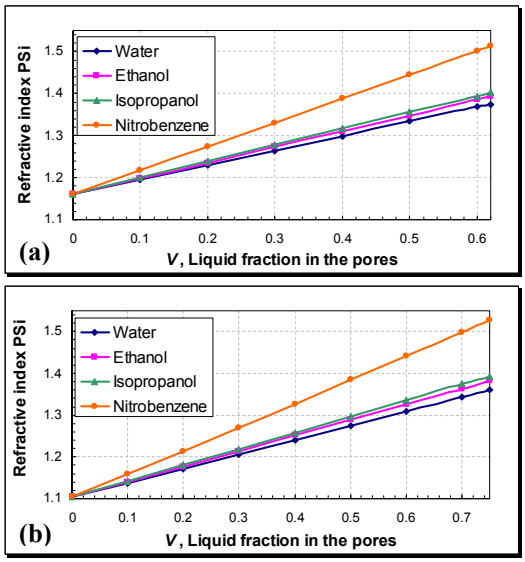

Figure 2. Calculated refractive index of oxidized PSi with (a) 62% and (b) 75% porosity as a function of ethanol liquid-filling fraction.

3.2 Porous Silicon Waveguide Mode Analysis

The PSi waveguide rib structure is assumed to consist of two porous silicon layers on a silicon substrate: an upper porous silicon layer (core) with a low porosity (high refractive index) on a lower cladding layer with high porosity (lower refractive index). RF module's *Mode analysis* study was performed on a cross-section in the *xy*-plane of a waveguide. Maxwell's equation is solved for the magnetic wave that propagates in the *z* direction and has the form:

$$H(x,y,z,t) = H(x,y)\cdot e^{j(wt-\beta z)} \qquad (4)$$

where ω is the angular frequency and β is the propagation constant,

$$\beta = n_{eff}\, 2\pi/\lambda . \qquad (5)$$

Guided modes exhibit an evanescent tail in the cladding and have an effective refractive index larger than the cladding materials (PSi cladding layer and air). A stationary linear direct solver (UMFPACK) is employed to solve the model and analyse the electromagnetic field of the guided modes. The maximum mesh size is set to 0.1 µm. Perfectly Matched Layers (PMLs) are used at the computational window boundaries to minimize errors in the calculations by eliminating reflections. The outer boundaries are defined as the scattering boundary condition. A full-vector analysis method is used which takes into account both polarizations. The simulated waveguide modes are quasi-TE or quasi-TM determined by the direction of their major field component. A free-space wavelength of 1.55 µm is used in all simulations.

The height of the core and of the cladding was chosen to be 1 and 3 µm. The width of the waveguide providing single-mode operation at the 1.55 µm wavelength is determined; the effective refractive indices of the lower guided modes are calculated for varying waveguide dimensions. In Fig. 3, the mode intensity profiles of the two lowest modes are shown for both polarizations for a waveguide with a cross-section of 2.2 µm x 1 µm. The effective mode index of these modes is plotted in Fig. 4 as a function of waveguide width.

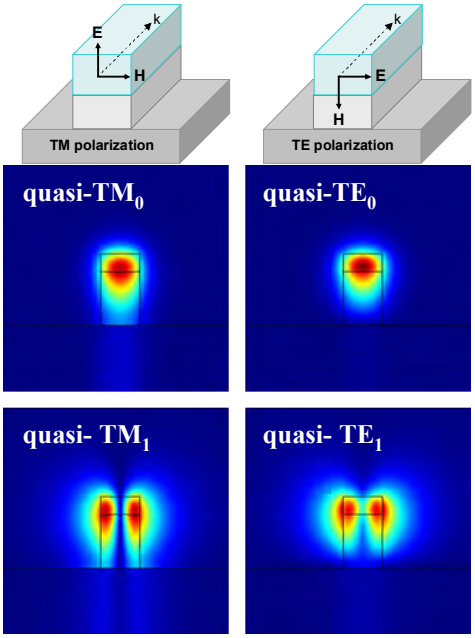

Figure 3. Mode intensity profiles of the first two order modes of the waveguide with 2.2 µm width for both polarizations.

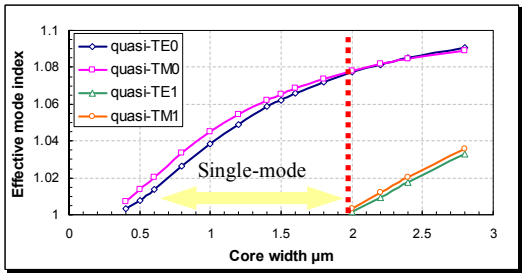

Figure 4. The effective refractive index as a function of the waveguide width, showing the core width region for single-mode operation.

The effect of vapour condensation in the PSi pores can be considered by using the third term in the Bruggeman effective-medium approximation (eq. 2) that incorporates the liquid-filling fraction *V*. The effect of increasing the liquid-filling fraction on the guided modes has been examined as a function of the waveguide width; as *V* increases, both core and cladding refractive indices change resulting in a different single-mode operation range. The plot showing the maximum width that ensures single-mode operation for liquid-filling fraction up to 0.6 is shown in Fig. 5. A waveguide core dimension of 1 µm x 1 µm is chosen as the PSi waveguide, as such features can be readily fabricated while ensuring waveguide single-

mode operation even in the presence of high-concentration organic vapour in the material pores.

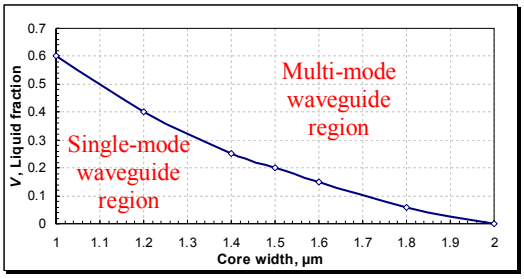

Figure 5. The liquid-filling volume fraction in the porous matrix that ensures single-mode operation of the PSi waveguides as a function of the waveguide width.

The effect of the height of the cladding layer on the effective index of the two lower order modes quasi-TM_0 and quasi-TE_0 is investigated. The change in the effective refractive index of these guided modes is plotted as a function of the cladding height in Fig. 6. It is found that a minimum height of 8 μm is required to minimize the mode coupling between the waveguide core and the silicon substrate.

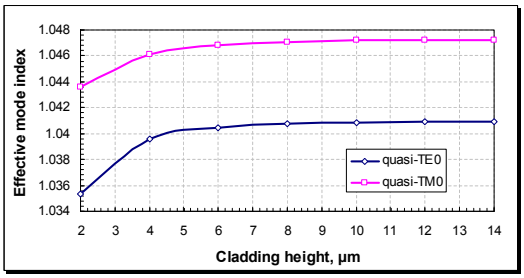

Figure 6. Effective indices of the first two modes as a function of cladding height.

3.3 PSi-Microring Sensor

The behaviour of a mirroring resonator consisting of a bus waveguide and a ring waveguide fabricated from PSi material is investigated. The simulations presented herein are based on a two-dimensional model in order to minimise the requirements in computational time and power, while providing some physical insight and initial results on the design of such structures.

Numeric port boundary conditions have been applied at the input and output of the bus waveguide, and two Boundary Mode Analysis studies have been performed for each port. A frequency domain study is used to calculate the mode propagation along the waveguide structure. For all simulations, the microring is assumed to have a radius of 21 μm and to be placed at a distance of 300 nm from the bus waveguide. The waveguide parameters are chosen appropriately to achieve resonant operating conditions around the 1.55 μm wavelength of interest. The propagation of the lower TM_0 mode along the microring structure is shown in Fig. 7 in the case of an off-resonant (λ=1.551 μm, Fig. 7a), and resonant operation (λ=1.543 μm, Fig. 7b).

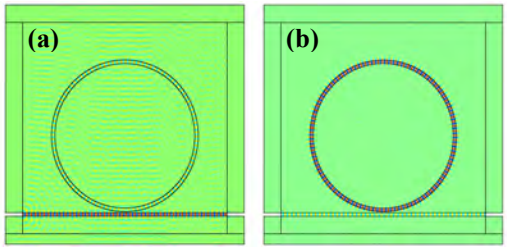

Figure 7. E_z field component for PSi-microring with 21μm radius, gap 300 nm at wavelength of (a) 1.551 μm and (b) 1.543 μm.

In order to compare the sensitivity of a PSi-microring sensor with a conventional microring sensor, simulations are performed for structures with different refractive indices of the surrounding medium. The surrounding medium can be gas or liquid, and acts as the cladding of the microring structure. The presence of specific molecules results in a change of the refractive index of the surrounding medium, and this in turn, results in a shift of the resonant wavelength. The value of this shift can provide an indication of the microring sensitivity to changes in their near environment, quantified as nanometers of resonance shift per unit of index change (nm/RIU). The transmission spectrum of the structure obtained for refractive indices of the surrounding medium of 1 and 1.01 are shown in Fig. 8. The shift in the resonance wavelength for such a 0.01 change in the refractive index of the surrounding medium was found to be 3.8 nm for conventional microring structure and 7 nm for a PSi-microring. Fig. 9 shows the wavelength shift in the microrings resonance as a function of change of the surrounding medium.

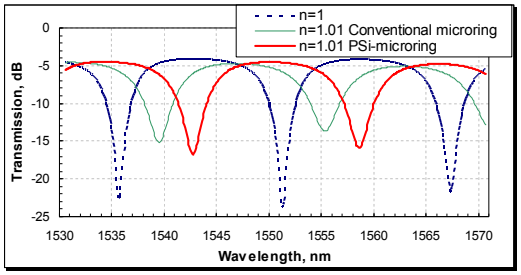

Figure 8. Simulated transmission for conventional and PSi-microrings due to change in 0.01 in the refractive index of the surrounding medium.

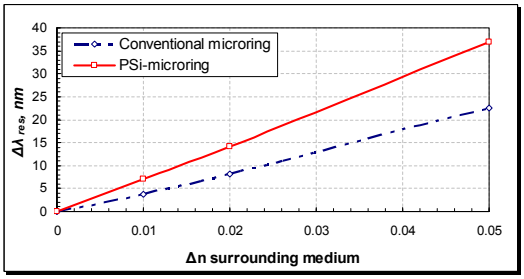

Figure 9. Simulated resonance peak shift as a function of the change of the refractive index of the surrounding medium.

The simulation results clearly demonstrate the potential of microring structures made from PSi over other material. An improved sensitivity of 700 nm/RIU is achieved for PSi-microring while a conventional microring resonator provides 380 nm/RIU for the same device parameters. Although microring resonator sensitivities as high as 490 nm/RIU have been reported for slot-waveguide geometry [24], where a nano-slot in the waveguide is used to enhance the light-matter interaction with the surrounding medium, our simulation results show the potential of obtaining similar or even better sensitivities with PSi-based structures. It needs to be noted however that full 3D simulations taking into account optical losses in the structure and further optimization of the microring design are required in order to obtain proper design parameters for a working device.

4. Conclusions

Porous silicon is an attractive material for use in sensing applications due to its porous nature which provides a large sensing surface. The infiltration of solvents or vapours into the material pores can efficiently sensed by monitoring the changes in light propagation inside appropriately designed PSi structures. In this work, theoretical studies of waveguides suitable for use as optical sensors and made of PSi are presented. Moreover, the use of PSi microring resonators in optical sensing is proposed and fundamental theoretical studies on such structures are presented. The initial simulation results indicate that a very good sensitivity is to be expected from even simple ring structures and clearly demonstrate the potential of such a technology.

5. References

1. J.-C. Vial, and J. Derrien, *Porous Silicon Science and Technology* (Springer Verlag, Berlin, 1995).
2. E. Lorenzo, C. J. Oton, N. E. Capuj, M. Ghulinyan, D. Navarro-Urrios, Z. Gaburro, and L. Pavesi, "Porous silicon-based rugate filters," Applied Optics **44**, 5415-5421 (2005).
3. L. De Stefano, L. Moretti, A. Lamberti, O. Longo, M. Rocchia, A. M. Rossi, P. Arcari, and I. Rendina, "Optical sensors for vapors, liquids, and biological molecules based on porous silicon technology," Nanotechnology, IEEE Transactions on **3**, 49-54 (2004).
4. A. M. Tinsley-Bown, L. T. Canham, M. Hollings, M. H. Anderson, C. L. Reeves, T. I. Cox, S. Nicklin, D. J. Squirrell, E. Perkins, A. Hutchinson, M. J. Sailor, and A. Wun, "Tuning the pore size and surface chemistry of porous silicon for immunoassays," Physica Status Solidi a-Applied Research **182**, 547-553 (2000).
5. J. Charrier, C. Lupi, L. Haji, and C. Boisrobert, "Optical study of porous silicon buried waveguides fabricated from p-type silicon," Materials Science in Semiconductor Processing **3**, 357-361 (2000).
6. J. Charrier, M. Kloul, P. Pirasteh, J. F. Bardeau, M. Guendouz, A. Bulou, and L. Haji, "Structural and optical studies of porous silicon buried waveguides: Effects of oxidation and pore filling using DR1 dyes," Optical Materials **30**, 431-437 (2007).
7. H. F. Arrand, T. M. Benson, A. Loni, R. Arens-Fischer, M. Kruger, M. Thonissen, H. Luth, and S. Kershaw, "Novel liquid sensor based on porous silicon optical waveguides," Ieee Photonics Technology Letters **10**, 1467-1469 (1998).

8. H. F. Arrand, T. M. Benson, A. Loni, R. Arens-Fischer, M. G. Krueger, M. Thoenissen, H. Lueth, S. Kershaw, and N. N. Vorozov, "Solvent detection using porous silicon optical waveguides," Journal of Luminescence **80**, 119-123 (1998).
9. P. Pirasteh, J. Charrier, Y. Dumeige, A. Chaillou, M. Guendouz, and L. Haji, "Study of porous silicon optical waveguides impregnated with organic dyes," Applied Surface Science **253**, 3440-3443 (2007).
10. T. Gao, J. Gao, and M. J. Sailor, "Tuning the response and stability of thin film mesoporous silicon vapor sensors by surface modification," Langmuir **18**, 9953-9957 (2002).
11. G. M. Ohalloran, M. Kuhl, P. J. Trimp, and P. J. French, "The effect of additives on the adsorption properties of porous silicon," Sensors and Actuators a-Physical **61**, 415-420 (1997).
12. J. O. Das, S. Dey, S. M. Hossain, Z. M. C. Rittersma, and H. Saha, "A hygrometer comprising a porous silicon humidity sensor with phase-detection electronics," Ieee Sensors Journal **3**, 414-420 (2003).
13. Z. M. Rittersma, A. Splinter, A. Bodecker, and W. Benecke, "A novel surface-micromachined capacitive porous silicon humidity sensor," Sensors and Actuators B-Chemical **68**, 210-217 (2000).
14. C. J. Oton, L. Pancheri, Z. Gaburro, L. Pavesi, C. Baratto, G. Faglia, and G. Sberveglieri, "Multiparametric porous silicon gas sensors with improved quality and sensitivity," Physica Status Solidi a-Applied Research **197**, 523-527 (2003).
15. M. Khardani, M. Bouaicha, and B. Bessais, "Bruggeman effective medium approach for modelling optical properties of porous silicon: comparison with experiment," Physica Status Solidi C - Current Topics in Solid State Physics, Vol 4 No 6 **4**, 1986-1990 (2007).
16. L. De Stefano, N. Rendina, L. Moretti, S. Tundo, and A. M. Rossi, "Smart optical sensors for chemical substances based on porous silicon technology," Applied Optics **43**, 167-172 (2004).
17. J. Gao, T. Gao, and M. J. Sailor, "Porous-silicon vapor sensor based on laser interferometry," Applied Physics Letters **77**, 901-903 (2000).
18. P. A. Snow, E. K. Squire, P. S. J. Russell, and L. T. Canham, "Vapor sensing using the optical properties of porous silicon Bragg mirrors," Journal of Applied Physics **86**, 1781-1784 (1999).
19. M. A. Anderson, A. Tinsley-Bown, P. Allcock, E. A. Perkins, P. Snow, M. Hollings, R. G. Smith, C. Reeves, D. J. Squirrell, S. Nicklin, and T. I. Cox, "Sensitivity of the optical properties of porous silicon layers to the refractive index of liquid in the pores," Physica Status Solidi a-Applied Research **197**, 528-533 (2003).
20. L. De Stefano, L. Moretti, I. Rendina, and A. M. Rossi, "Quantitative optical sensing in two-component mixtures using porous silicon microcavities," Physica Status Solidi a-Applied Research **201**, 1011-1016 (2004).
21. S. E. Letant, and M. J. Sailor, "Molecular identification by time-resolved interferometry in a porous silicon film," Advanced Materials **13**, 335-338 (2001).
22. T. Hutter, I. Presiado, S. Ruschin, and D. Huppert, "Protic Properties of Water Confined in the Pores of Oxidized Porous Silicon Studied by Excited-State Proton Transfer from a Photoacid," Journal of Physical Chemistry C **114**, 2341-2348 (2010).
23. C. Mazzoleni, and L. Pavesi, "Application to Optical-Components of Dielectric Porous Silicon Multilayers," Applied Physics Letters **67**, 2983-2985 (1995).
24. J. T. Robinson, L. Chen, and M. Lipson, "On-chip gas detection in silicon optical microcavities," Opt. Express **16**, 4296-4301 (2008).